Applied Catalysis B: Environmental 234 (2018) 357–364

Contents lists available at ScienceDirect

Applied Catalysis B: Environmental

journal homepage: www.elsevier.com/locate/apcatb

Immunity of the Fe-N-C catalysts to electrolyte adsorption: Phosphate but not perchloric anions

Yang Hu*, Jens Oluf Jensen, Chao Pan, Lars Nilausen Cleemann, Illia Shypunov, Qingfeng Li*

Department of Energy Conversion and Storage, Technical University of Denmark, Elektrovej 375, DK-2800 Kgs. Lyngby, Denmark

ARTICLE INFO

Keywords:
Oxygen reduction
Catalyst
Fuel cell
Anion
Poison

ABSTRACT

Non-precious metal catalysts (NPMCs), particularly the type based on carbon-supported FeN_x functionalities (Fe-N-C) are a very promising material for replacing the rare and costly platinum-based catalysts in polymer electrolyte membrane fuel cells (PEMFCs). Evaluation of these materials is most often carried out, like for Pt-based catalysts, in dilute perchloric acid by assuming its non-adsorbing nature on the active sites. The assumption is however not true. In this work, a typical Fe-N-C catalyst was first synthesized by high-pressure pyrolysis in the presence of a carbon support and thoroughly characterized in terms of morphology, structure and active site distribution. The subsequent electrochemical characterization of the catalyst shows strong adsorption and poisoning effect of, in addition to the known Cl^-, perchloric anions on the oxygen reduction reaction (ORR) activity. On the contrary, phosphate anions exhibit negligible poisoning effect on the catalyst activity. At 0.8 V vs. RHE, the ORR activity of the catalyst is found to decrease in the order of H_3PO_4 (8.6 mA mg^{-1}) > H_2SO_4 (5.3 mA mg^{-1}) > $HClO_4$ (3.1 mA mg^{-1}) > HCl (0.7 mA mg^{-1}). The results suggest potential applications of NPMC in high-temperature PEMFCs based on phosphoric acid doped polymer membranes, where high-loading platinum catalysts are currently used. As demonstrated in the low current density range of high-temperature PEMFCs, the catalyst shows a comparable performance to the Pt/C catalysts.

1. Introduction

Energy is undoubtedly one of the key elements for a sustainable society. The transition from fossil fuels to renewable energy sources has been an on-going process for many countries due to the increasing energy consumption and the concern for environmental deterioration. Recently, several countries such as Germany, Norway, and France have announced different timetables for a ban on sales of fossil fuel cars [1]. China, which has the world's largest car market, is currently developing a timetable for a similar ban [2]. Obviously, in the future, techniques that can produce, convert or store renewable energy will play a more significant role in our societies.

Fuel cells are a highly efficient and environmentally benign technology to convert chemical energy directly into electrical energy. Among several types of fuel cells under active development, the polymer electrolyte membrane fuel cell (PEMFC) is regarded as a promising power source for fossil fuel-free cars and other portable or stationary applications [3,4]. Thus far, platinum-based nanocatalysts are the state-of-the-art for both the anode and cathode of PEMFCs. However, the high cost and limited availability of platinum are a big issue for the wide adoption of this technology [5,6]. Besides, regarding high-temperature PEFMCs that typically employ a phosphoric acid-doped polybenzimidazole (PBI) membrane, the strong adsorption of phosphates on platinum is another major issue, which significantly decreases the catalyst activity and the overall cell performance [7, [9–13]]. In order to replace platinum-based catalysts in PEFMCs, especially on the cathode side, various non-precious metal catalysts (NPMCs) have been developed. Among them, composite materials comprising porous carbon supported Fe-N functionalities (referred to as Fe-N-C catalysts) exhibit the best activity. and are typically synthesized by pyrolyzing precursors containing iron, nitrogen, and carbon at temperatures ranging from 600 to 1000 °C [9–13].

The state-of-the-art PEMFC performance based on Fe-N-C catalysts matches that of Pt/C at low and even medium current densities, though the needed catalyst loading is typically 3–6 times higher [14,15]. At the cell voltage of 0.8 V, the performance of this type catalyst, determined by extrapolating from the Tafel plot, was reported to reach a volumetric current density of 99 A cm^{-3} in 2009 [16] and 230 A cm^{-3} in 2011 [17]. The recent breakthrough was from a MOF-based nanofibrous catalyst, which showed the activity of 450 A cm^{-3} at the cell voltage of 0.8 V, which exceeded the newly updated 2017/2020 U.S. Department of Energy (DOE) target of 300 A cm^{-3} [15].

* Corresponding authors.
E-mail addresses: yanhu@dtu.dk (Y. Hu), qfli@dtu.dk (Q. Li).

https://doi.org/10.1016/j.apcatb.2018.03.056
Received 15 November 2017; Received in revised form 19 February 2018; Accepted 18 March 2018
Available online 19 March 2018

Like for platinum-based catalysts, the NPMC is often evaluated by the rotating disk electrode test using dilute perchloric acid or sulfuric acid as the electrolyte. As chloride and phosphate anions are well known to adsorb on Pt, [18–21] perchloric and sulfuric acids are considered to be weakly adsorbing electrolytes that have been used to simulate the role of the Nafion ionomer in PEMFCs [22,23]. Trace contaminations in the testing $HClO_4$ electrolyte such as chloride, nitrate in ppb to ppm levels show significant effects on the ORR activity of the Pt catalysts [21,23–27]. It is, therefore, a general practice in the electrochemical characterization of ORR catalysts that cell glassware, rotator shafts, electrode tips and electrolytes undergo a very careful cleaning procedure to avoid these impurities. For Fe-N-C catalysts, they are always assumed to be immune to anion adsorption and characterized usually in dilute perchloric acid or sulfuric acid [13,28]. The effect of anions on the ORR performance of Fe-N-C catalysts, except for the strongly Fe-chelating species such as CN^- and SCN^- [18–21], however, have not been carefully investigated. This work is devoted to such a study focusing on common anions including ClO_4^-, HSO_4^-, Cl^-, and $H_2PO_4^-$. The chloride ion is a common impurity originating from contaminations of the electrolyte or the glassware or from the reference electrode such as a saturated calomel electrode (SCE) or an Ag/AgCl electrode [29,30]. Phosphate is of special interest in relation to phosphoric acid fuel cells (PAFC) and high-temperature PEMFC, which both contain phosphoric acid [31]. These cells are currently based on platinum catalysts at a significantly higher loading, as a consequence of the strong phosphate adsorption of the platinum surface [32]. It is, therefore, a more critical issue for evaluation and utilization of NPMCs in PAFC and HT-PEMFC. In this regard, Li et al. studied the effect of phosphate ions on the catalytic activity in $HClO_4$ and reported good tolerance of an Fe-derived catalyst at concentrations of up to 5.0 M H_3PO_4 [33].

In this work, a typical Fe-N-C catalyst was first synthesized by high-pressure pyrolysis in the presence of a carbon support and characterized in terms of the morphology, structure and active site distribution. The catalyst was then used to probe the effect of four common anions, i.e. ClO_4^-, HSO_4^-, $H_2PO_4^-$ and Cl^- on its ORR performance. The measured ORR activities followed the sequence of H_3PO_4 > H_2SO_4 > ClO_4 > HCl. Surprisingly, in addition to well-known poisoning Cl^-, the ClO_4^- also had a strong poisoning effect for Fe-N-C catalysts, whereas that of HSO_4^- was more gentle. The adsorption of $H_2PO_4^-$ was, on the other hand, negligible on the catalyst. As a result, the catalyst exhibited a better catalytic activity towards the ORR in phosphoric acid than in perchloric acid, which indicated its promising application in high-temperature PEMFCs. As demonstrated, the catalyst did show excellent performance in high-temperature PEMFC tests, which, in the low current density range, is comparable to Pt/C catalysts.

2. Experimental

2.1. Catalyst synthesis

The catalyst (named as BP-FeNC hereafter) was synthesized by pyrolyzing the precursors cyanamide (NH_2CN, 99%, Sigma-Aldrich), ferrocene ($Fe(C_5H_5)_2$, 98%, Sigma-Aldrich) and Black Pearls 2000 carbon black (BP, CABOT) at 750 °C in an autoclave (made from stainless steel, 2.3 mL). Specifically, 300.1 mg of cyanamide, 33.7 mg of ferrocene and 51.2 mg of BP were thoroughly mixed and transferred into a quartz holder in the autoclave. The autoclave was transferred to an Ar-filled glove box and closed there. After that, the autoclave was taken out of the glovebox and placed in a tube-furnace with Ar flow for the heat-treatment (the Ar flow was for protecting the autoclave from oxidation at high temperatures). The tube furnace was heated from room temperature to 750 °C at a rate of 10 °C min^{-1} and maintained at 750 °C for 1 h, after which the autoclave was moved away from the heating zone to achieve fast cooling. After opening the autoclave at room temperature, a black powder of 38.0 wt % of the initial precursors mass was collected. After subtraction of the mass of carbon black, 65.3 wt% of the product was newly formed phases. The product was leached in 1.0 M H_2SO_4 at room temperature in an ultrasonic bath for 5 h to remove unstable phases, and then it was washed thoroughly with Milli-Q water (close to 100 °C) and dried at 95 °C for 5 h. At last, the catalyst was heat-treated again under Ar flow (99.999%) at 800 °C for 1 h.

2.2. Physical characterizations

Transmission electron microscopy (TEM) and high-angle annular dark-field scanning transmission electron microscopy (HAADF-STEM) images were obtained with an FEI Titan Analytical 80-300ST TEM at 300 kV. Nitrogen sorption isotherms were measured at 77 K with a Micromeritics ASAP 2020. Before analysis, the catalysts were degassed in vacuum at 200 °C for 24 h. The surface area was determined using the BET method based on adsorption data in the relative pressure (P/P°) range of 0.06 to 0.14. The pore size distribution was determined using the BJH method. Powder X-ray diffraction (XRD) measurements were performed with a MiniFlex 600 X-ray diffractometer (Rigaku) using a Cu Kα (λ = 1.5405 Å) radiation source. X-ray photoelectron spectroscopy (XPS) measurements were carried out on a Thermo Scientific K-Alpha + X-ray Photoelectron Spectrometer with an Al Kα X-ray monochromator. Survey scans were obtained using a pass energy of 200 eV, while high-resolution scans of specific elements were obtained using a 50 eV pass energy. The binding energy shift was checked by carrying out a valence scan. Data quantification was performed using the Avantage program. Inductively coupled plasma-optical emission spectroscopy (ICP-OES) analysis was conducted using a Varian Vista-MPX. For the ICP-OES analysis, the BP-FeNC catalyst was first heat-treated in air flow at 800 °C to remove the carbon component. The residue was then dissolved in a mixture of trace metal-grade concentrated hydrochloric and nitric acids, which was diluted with Milli-Q water for the analysis.

2.3. Electrochemical measurements

Electrochemical measurements were conducted using a VSP multichannel potentiostat from Biologic. $HClO_4$, H_2SO_4, H_3PO_4 and HCl solutions at pH 1.0 were prepared by diluting high-purity concentrated chemicals, i.e. $HClO_4$ (70%, Aldrich), H_2SO_4 (95–97%, Sigma-Aldrich), H_3PO_4 (≥85%, Fluka) and HCl (37%, Sigma-Aldrich), respectively. BP-FeNC catalyst inks were prepared by ultrasonically dispersing 5.0 mg catalyst in a mixture consisting of 40 μL Nafion solution (5 wt %) and 385.17 μL formic acid (≥95%). Pt/C catalyst inks (20 wt%, Johnson Matthey) was prepared by dispersing 5 mg of catalyst in a mixture of 2460 μL formic acid (≥95%), 50 μL Nafion solution (5 wt %) and 40 μL Milli-Q water. A specific amount of ink was cast onto a rotating disk electrode (RDE, 0.196 cm^2, Pine Research Instrumentation) or rotating ring-disk electrode (RRDE) (0.196 cm^2, Pine Research Instrumentation) to reach the required catalyst loading. A standard three-electrode cell was employed for the measurements, which incorporated the RDE/RRDE as the working electrode, a graphite rod (99.995% trace metals basis) as the counter electrode and a daily prepared reference hydrogen electrode (RHE) as the reference electrode. The filling electrolyte in the RHE was the same as that in the main compartment, which avoided the possible contamination from the reference electrodes, e.g. SCE or Ag/AgCl. The RHE was calibrated before each test. Both the reference electrode and the counter electrode were separated from the working electrode compartment using porous glass frits. All glassware was cleaned in Piranha solution and rinsed with hot Milli-Q water at least three times before use. Ultra-high purity O_2 (99.999%) and Ar (99.999%) were used in the measurements. All ORR curves have been corrected for the capacitive current and the solution resistance, with the latter being measured by electrochemical impedance spectroscopy (EIS), which was recorded at open circuit potential by applying an AC signal with 10 mV amplitude over the frequency range from 100 kHz to

0.1 Hz. Tafel plots shown in Fig. 3b and e were calculated from the corresponding ORR polarization curves after mass-transport correction by the equation

$$\frac{1}{i} = \frac{1}{i_k} + \frac{1}{i_l} \quad (1)$$

where i_k is the kinetic current density, i_l is the diffusion limiting current density, and i is the measured current density. For the consistency, in this work, i_l was defined as the current density at 0.3 V for each curve. Regarding RRDE tests, the ring potential was held at 1.2 V, while the disc potential was scanned. The H_2O_2 collection coefficient for the ring was 0.254, determined by measurements in a $K_3Fe(CN)_6$ solution, in good agreement with the manufacturer value. The following equation was used to calculate the $\%H_2O_2$ (the percentage of H_2O_2 released during ORR),

$$\%H_2O_2 = 100\frac{2I_R/N}{I_D + (I_R/N)} \quad (2)$$

where I_D is the Faradaic current at the disk, I_R the Faradaic current at the ring and N is the H_2O_2 collection coefficient at the ring. All measurements were carried out at room temperature. Considering the following equilibria for H_3PO_4 solutions,

$$H_3PO_4 + H_2O \rightleftharpoons H_3O^+ + H_2PO_4^-(pK_{a1} \approx 2.16) \quad (3)$$

$$H_2PO_4^- + H_2O \rightleftharpoons H_3O^+ + HPO_4^{2-}(pK_{a2} \approx 7.21) \quad (4)$$

$$HPO_4^{2-} + H_2O \rightleftharpoons H_3O^+ + PO_4^{3-}(pK_{a3} \approx 12.32) \quad (5)$$

in the present study in acidic media, only $H_2PO_4^-$ is of significance. HPO_4^{2-} will be dominantly present in neutral while PO_4^{3-} is present in basic media.

2.4. Fuel cell tests

Catalyst inks were prepared by mixing the catalyst (BP-FeNC, 60 wt % Pt/C or 20 wt % Pt/C) with a specific amount of PBI/formic acid solution, as specified in Table 1. The gas diffusion layer (GDL) was Freudenberg H23C2, a commercial carbon cloth coated with a carbon microporous layer (MPL) on one side. The cathodes were prepared by spraying the catalytic ink over the MPL. The anodes were commercial Pt-based electrodes with a loading of 1.6 $mg_{Pt}\,cm^{-2}$ from Danish Power Systems. The membrane electrode assemblies (MEAs) were constructed by assembling an H_3PO_4-doped PBI membrane (80 μm thick, polymer molecular weight of ca. 78,000) between the electrodes without hot pressing. High-temperature PEMFC single cells with an active area of 1 cm^2 were used for all the tests. Polarization curves were recorded by scanning the cell voltage from OCV down to 0.1 V at a scan rate of 1 $mV\,s^{-1}$ using the staircase cyclic voltammetry. Given that the focus of fuel tests was on the catalyst performance evaluation, O_2, instead of air, was used. All the tests were carried out at ambient pressure and 160 °C with non-humidified gasses (H_2/O_2).

3. Results and discussion

The BP-FeNC catalyst was synthesized by pyrolyzing cyanamide, ferrocene, and BP in an autoclave at 750 °C. The morphology and structure of the catalyst are shown in Fig. 1. As revealed by the SEM image (Fig. 1a), it has a similar morphology to BP (Fig. S1), consisting of mainly sub-100 nm particles. Typical TEM (Fig. 1b) and HAADF-STEM (Fig. 1c) images exhibit consistent phase contrast across the catalyst, signifying the absence of metal particles in the catalyst. This was further confirmed by XRD analysis. As depicted in Fig. 1d, the XRD pattern of BP-FeNC shows no crystalline phase other than the partly graphitized carbon, similar to BP. The pore structure of the catalyst was studied by BET analysis, showing a specific surface area of 565 $m^2\,g^{-1}$, lower than BP (1473 $m^2\,g^{-1}$). The pore size distribution is centered at 4 nm and 30 nm, indicating the mesoporous structure of the newly formed phases in the catalyst. In a previous work using the similar autoclave approach, we synthesized a catalyst with a very different structure which were hollow spheres of graphitic layer encapsulated iron carbide nanoparticles.[30] The main difference in the synthesis between this work and the previous one is the addition of the BP carbon support in the precursor, which leads to almost no metal particle formation in the obtained BP-FeNC catalyst. Besides BP, we have tried other carbon supports to synthesize the catalyst, including Ketjenblack EC-600J, graphitized Vulcan XC-72, and multi-walled carbon nanotubes (MW-CNTs). In all those syntheses, however, certain amounts of metal crystals were always found in the final catalysts, especially for the syntheses using graphitized Vulcan carbon and MW-CNTs, as revealed by XRD analysis (Fig. S2). Given that the BET surface areas of these four carbon materials decrease in the sequence of BP > Ketjenblack > graphitized Vulcan XC-72 > MW-CNTs [34], the formation of metal particles is assumed relative to the pore structure of the carbon support. Cyanamide and ferrocene have a melting point of 44 °C and 172 °C, respectively. When the temperature was raised during synthesis, the two precursors likely melted and redistributed in the pores or on the surface of carbon supports, facilitating the distribution of newly formed active carbon or FeN_x phases. In the case of supports with lower specific surface areas such as MW-CNTs, the precursor would probably tend to form iron-rich particles during the pyrolysis at higher temperatures.

To explore the active sites on the catalyst, XPS (Fig. 2a–c) and STEM-EDS elemental mapping (Fig. 2d–f) analysis were conducted. The XPS spectra revealed the near-surface elemental contents in the catalyst, which was 93.33 at.% of C, 3.07 at.% of N, 3.24 at.% of O, and 0.27 at.% of Fe. Peak fitting of the N 1 s spectrum reveals mainly pyridinic N (42.24%, at 398.33 eV) and graphitic N (39.44%, at 400.81 eV), alongside a small amount of oxidized N (15.92%, at 402.87 eV) and pyrrolic N (2.39%, at 399.45 eV). Although no consensus has been achieved thus far regarding the role of specific N species in FeN_x active site structure, the importance of pyridinic N and graphitic N have been widely assumed.[14,35,36] The bulk iron content of BP-FeNC was determined by inductively coupled plasma-optical emission spectroscopy (ICP-OES) analysis and was found to be 1.04 wt %. Despite such a low iron content in the catalyst, elemental mapping images from the STEM-EDS analysis clearly show the uniform distribution of iron species across the catalyst (Fig. 2d–f), suggesting a uniform distribution of FeN_x sites. In summary, we have synthesized a quite typical Fe-N-C catalyst, which contains uniformly distributed FeN_x sites but no metal particles.

Next, the ORR performance of the catalyst was evaluated in four electrolytes: $HClO_4$, H_2SO_4, H_3PO_4, and HCl. They were prepared with the same pH value of 1.0 to ensure the same acidity. In order to avoid any other anion sources, the electrochemical cell was thoroughly cleaned before each test, and a RHE, instead of a SCE or Ag/AgCl electrode, was used for all the measurements. For comparison, a commercial Pt/C was also tested and the result is discussed first. As shown in Fig. 3a–c, the ORR activities of Pt/C differ significantly in these four electrolytes. The mass-specific activity (at 0.9 V) decreases in the order of $HClO_4$ (304.2 $mA\,mg_{Pt}^{-1}$) > H_2SO_4 (123.1 $mA\,mg_{Pt}^{-1}$) > H_3PO_4 (13.2 $mA\,mg_{Pt}^{-1}$) > HCl (~0 $mA\,mg_{Pt}^{-1}$). The smaller ORR diffusion limiting current in H_3PO_4 was due to its slightly different physical

Table 1
Experimental parameters for high-temperature-PEMFC tests.

	Catalyst loading ($mg\,cm^{-2}$)	PBI/catalyst/H_3PO_4 (wt%) in the cathode	Gas flow ($mL\,min^{-1}\,cm^{-2}$): O_2/H_2
60 wt% Pt/C	2.7 (1.6_{Pt})	1/35.0/0	20/20
20 wt% Pt/C	4.4 (0.88_{Pt})	1/8.8/10	20/20
BP-FeNC	7.8	1/8.5/10	20/20

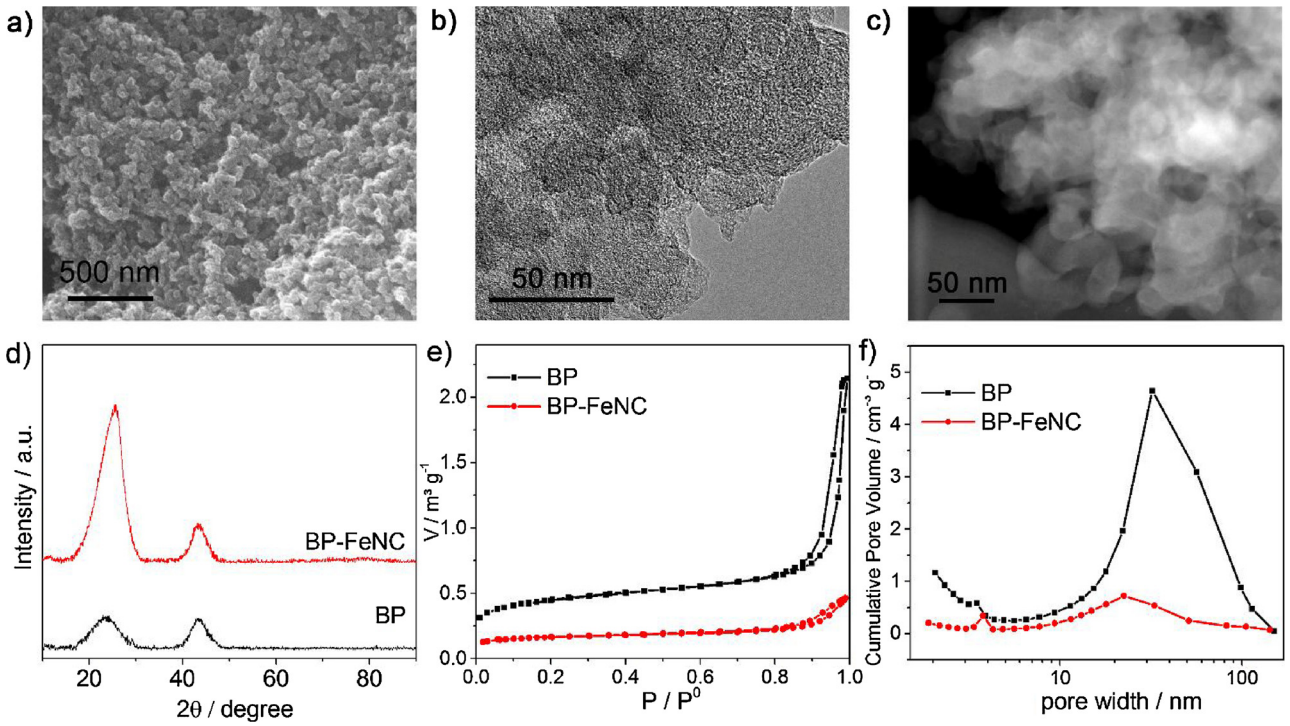

Fig. 1. Structural characterization of the BP-FeNC catalyst. a) SEM, b) TEM, and c) HAADF-STEM images of BP-FeNC. d) XRD patterns of BP and BP-FeNC. e) Nitrogen adsorption and desorption isotherms of BP and BP-FeNC. The BET surface areas of BP and BP-FeNC are 1473.0 and 565.3 $m^2 g^{-1}$, respectively. f) BJH pore-size distribution of BP and BP-FeNC derived from BET measurements.

properties, including the higher electrolyte viscosity, lower oxygen solubility and smaller oxygen diffusion coefficient. This can be seen from the Levich equation: $i_l = 0.62\ nFAD^{2/3}\omega^{1/2}\nu^{-1/6}C^*$, where i_l is the limiting current, F is the Faraday constant, A is the surface area of the electrode, D is the diffusion coefficient of O_2 in the electrolyte, ω is angular frequency of rotation, ν is the kinetic viscosity of the electrolyte, and C^* is the bulk concentration of O_2 in the electrolyte. As long as there is no anion adsorption or poisoning effect from the electrolyte, the slightly different properties of the electrolyte will not affect the measured ORR curves in the kinetic and mixed kinetic - diffusion region and hence will not influence the ORR activities (which is shown in Fig. 4a). The smaller limiting current in HCl, however, is caused

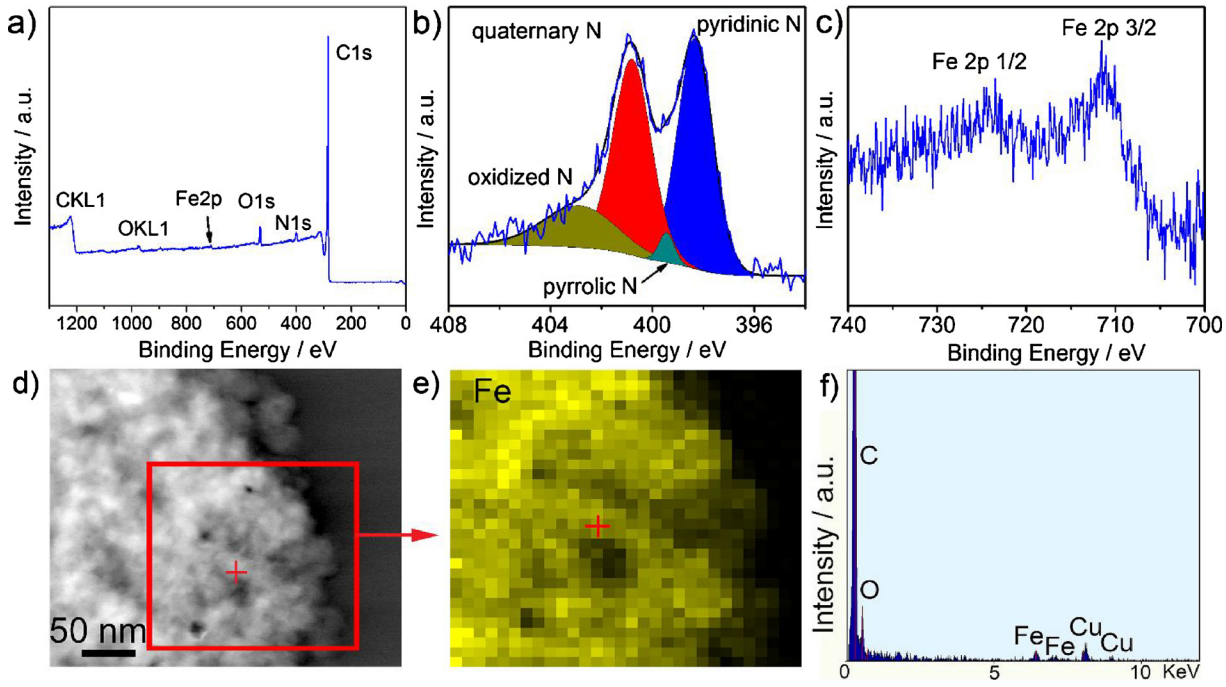

Fig. 2. Active site exploration of the BP-FeNC catalyst. a) XPS survey spectrum. b,c) High-resolution XPS spectra of N 1 s with the peak deconvolution (b) and Fe 2p (c). d–f) HAADF-STEM image (d) and the corresponding elemental mapping of Fe-K (e) as well as the EDS point analysis on the spot marked with red crosses on the images (f). The Cu signal originates from the TEM grid (For interpretation of the references to colour in this figure legend, the reader is referred to the web version of this article).

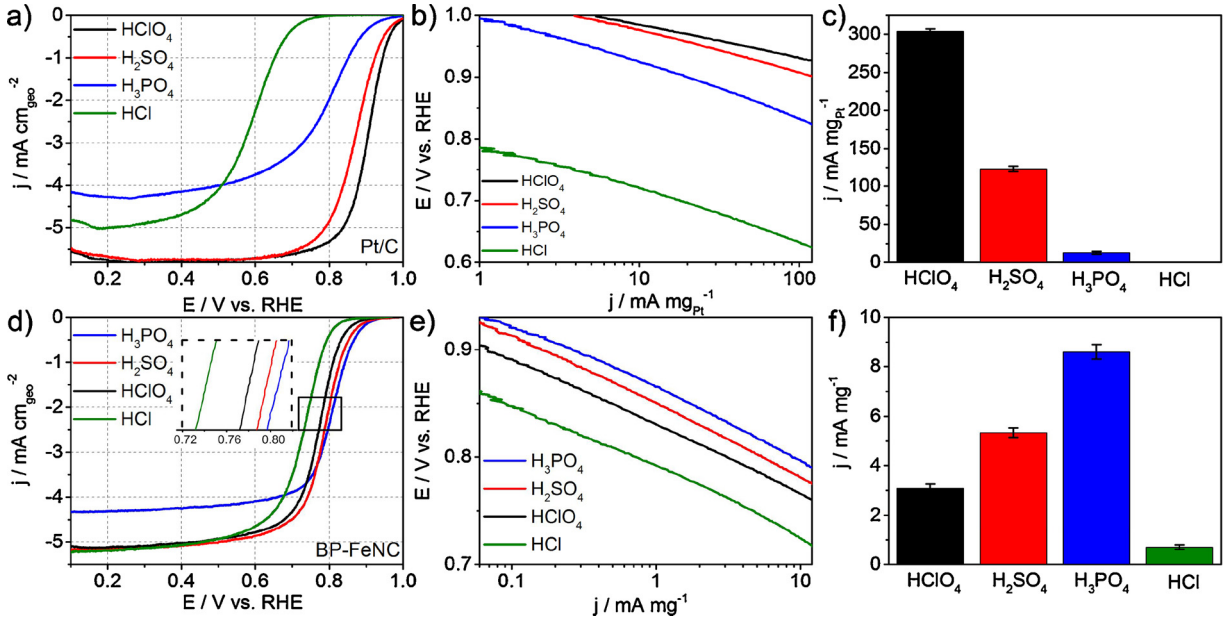

Fig. 3. ORR characterizations of Pt/C and BP-FeNC in pH 1.0 $HClO_4$, H_2SO_4, H_3PO_4 and HCl solutions. a–c) ORR polarization curves (anodic scans), Tafel plots, and mass-specific activities (at 0.9 V) of 20 wt% Pt/C (from Johnson Matthey). Catalyst loading: 20 $\mu g_{Pt}\,cm^{-2}$; Rotation rate: 1600 rpm; Scan rate: 10 $mV\,s^{-1}$. d–f) ORR polarization curves (cathodic scans), Tafel plots and mass-specific activities (at 0.8 V) of BP-FeNC. Catalyst loading: 600 $\mu g\,cm^{-2}$; Rotation rate: 1600 rpm; Scan rate: 10 $mV\,s^{-1}$. Error bars in (c) and (f) show the standard deviation of each data point from at least three independent measurements. To minimize the error, only the ORR currents below 80% of the diffusion limiting currents were used in Tafel analysis.

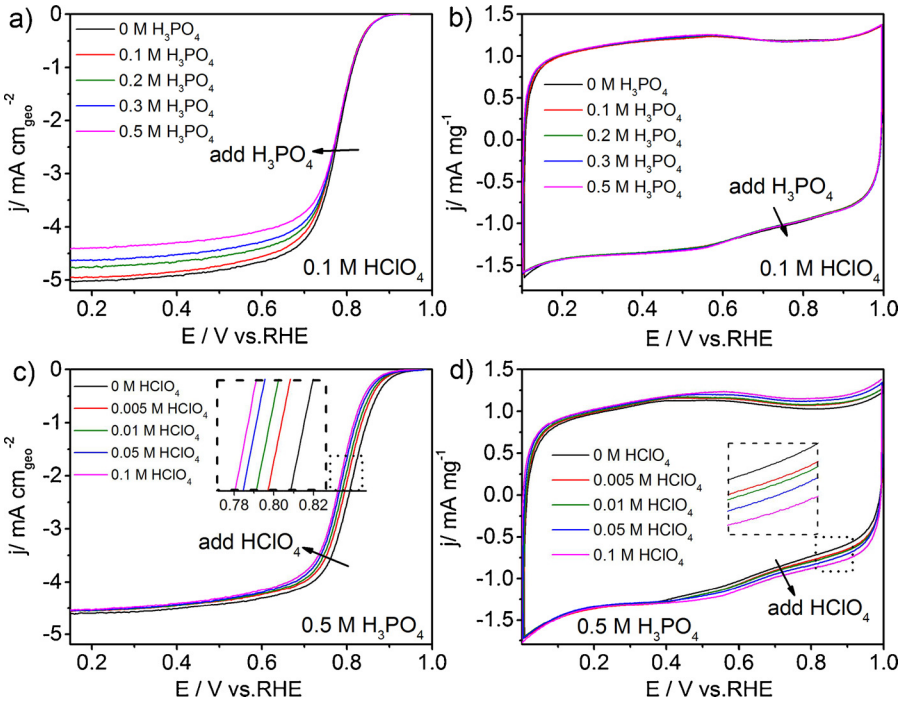

Fig. 4. a) ORR polarization curves (cathodic scans) of BP-FeNC in 0.1 M $HClO_4$ with the addition of various amounts of H_3PO_4. b) The corresponding CVs of BP-FeNC in the Ar-saturated electrolytes. c) ORR polarization curves (cathodic scans) of BP-FeNC in 0.5 M H_3PO_4 with the addition of various amounts of $HClO_4$. d) The corresponding CVs of BP-FeNC in the Ar-saturated electrolytes. Catalyst loading: 600 $\mu g\,cm^{-2}$; Scan rate: 10 $mV\,s^{-1}$; Rotation rate for ORR curves: 1600 rpm.

mainly by the severe blocking effect of Cl^- on Pt. [21,30,33,37] The detrimental effect of anions on the ORR performance of Pt/C catalysts is well-known and has been extensively studied. It can be explained by the strong chemisorption of anions on the Pt surface [21,38–43]. They are present on the Pt surface in the inner Helmholtz plane, generating the so-called "blocking effect", the extent of which is potential dependent (resulting in the typical two Tafel slopes, as shown in Fig. S3 and Table S1) and varies with different Pt crystal facets [44–48]. Concerning Pt nanoparticles as in the Pt/C catalyst, which are rich of low-index facets (e.g. 100, 110, and 111), the observed performance sequence mainly reflects the adsorption strength of these anions on the low-index facets, i.e. ClO_4^- < HSO_4^- < H_2PO4^- < Cl^- [21,42,44,49].

As to the BP-FeNC catalyst, the obtained results were significantly different (Fig. 3d–f). From the comparison between Fig. 3a and d, one can see the BP-FeNC is less sensitive to anions than Pt/C, but the poisoning effect is still quite significant. The half-wave potential shift is 10 mV from H_3PO_4 to H_2SO_4, 34 mV from H_3PO_4 to $HClO_4$, and further increases to 74 mV in HCl. Accordingly, the mass-specific activity (at 0.8 V) decreases from 8.6 mA mg^{-1} in H_3PO_4 to 5.3 mA mg^{-1} in H_2SO_4, to 3.1 mA mg^{-1} in $HClO_4$, and further down to 2.8 mA mg^{-1} in HCl, representing a 38%, 64% and 92% activity drop in H_2SO_4, $HClO_4$ and HCl, respectively. As discussed above, the slightly different physical

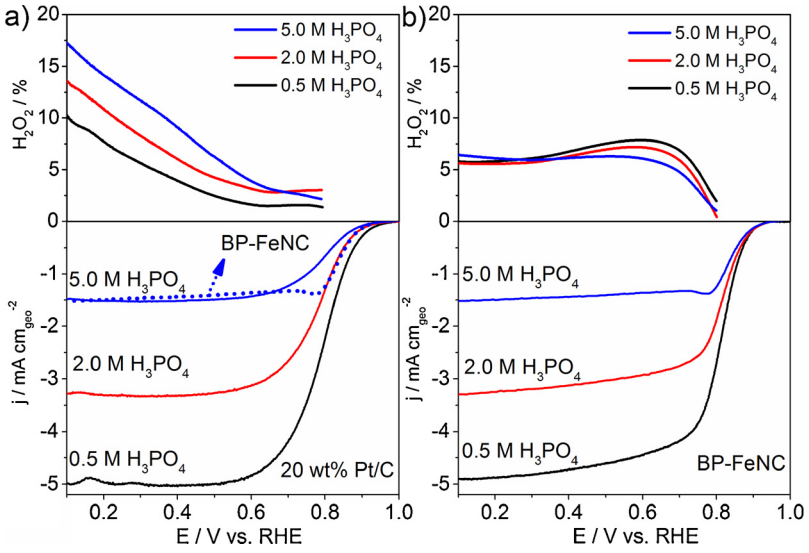

Fig. 5. a) ORR polarization curves (cathodic scans, bottom) and H_2O_2 yield plots (top) of 20 wt% Pt/C in H_3PO_4 solutions of different concentrations. Catalyst loading: 20 $\mu g_{Pt}\,cm^{-2}$; Rotation rate: 1600 rpm; Scan rate: 10 $mV\,s^{-1}$. For comparison, the ORR curve of BP-FeNC in 5.0 M H_3PO_4 (the dotted line) is also included. b) ORR polarization curves (cathodic scans, bottom) and H_2O_2 yield plots (top) of BP-FeNC in H_3PO_4 solutions of different concentrations. Catalyst loading: 600 $\mu g\,cm^{-2}$; Rotation rate: 1600 rpm; Scan rate: 10 $mV\,s^{-1}$.

properties of the H_3PO_4 solution will not affect the measured ORR performance. Hence, the only reasonable explanation is the effect of anion adsorption on the catalyst, with the adsorption strength in the order of $H_2PO_4^-$ < HSO_4^- < ClO_4^- < Cl^-. To check if this is a common property for this type of catalyst, we also tested a commercial Fe-N-C catalyst (NPC-2000 from Pajarito Powder), which showed similar results, as shown in Fig. S4.

The poisoning effect of ClO_4^- on the catalyst was further confirmed by two sets of control experiments. One was testing the catalyst in $HClO_4$ and inspecting the ORR activity change with the addition of various amounts of H_3PO_4, the other was done in a reverse manner, i.e. testing in H_3PO_4 with the addition of $HClO_4$. As the starting point, 0.1 M $HClO_4$ and 0.5 M H_3PO_4 were used since they had similar pH values close to 1. Regarding the tests in 0.1 M $HClO_4$ with various amounts of H_3PO_4 (Fig. 4a), the ORR curves show almost no shift in the kinetic region (0.8–0.95 V) with the addition of H_3PO_4 up to 0.5 M, suggesting the poisoning effect of $H_2PO_4^-$ is negligible on the catalyst. Besides, as aforementioned, the results also indicate the changed physical properties of the electrolyte by adding 0.5 M H_3PO_4 will not affect the ORR curves in the kinetic and mixed kinetic-diffusion region. On the other hand, the tests in 0.1 M H_3PO_4 with various amounts of $HClO_4$ show very different results, as depicted in Fig. 4c. The almost unchanged limiting currents of the ORR curves indicate the viscosity, oxygen solubility, and diffusion coefficient are largely unaffected by the addition $HClO_4$ up to 0.1 M. Meanwhile, however, the ORR curves shifted negatively with the addition of $HClO_4$. The half-wave potential shift was 11 mV with the presence of only 0.005 M $HClO_4$, which further increased to 17 mV, 24 mV, and 28 mV for 0.01 M, 0.05 M and 0.1 M $HClO_4$, respectively, confirming the poisoning effect of ClO_4^- on the catalyst. Alongside the changing in ORR activity, the addition of $HClO_4$ also caused the change of CVs of the catalyst. As shown in Fig. 4d, the CV intensities (i.e. the capacitance current) gradually increase with the addition of $HClO_4$, which means the addition of $HClO_4$ increases the electrochemical pseudocapacitance of the catalyst surface, a sign for specifically adsorbed ions (ClO_4^- in this case) on the catalyst surface [50]. On the contrary, as shown in Fig. 4b, the CVs of the catalyst exhibit no obvious change with the addition of H_3PO_4, suggesting the adsorption of $H_2PO_4^-$ on the catalyst is negligible.

It's been widely assumed in literature that Fe-N-C catalysts are immune to anions, except for several Fe-related strong poisons such as CN^- and SCN^- [28,51]. Obviously, this is not true on the basis of results from this work. Particularly, perchloric acid, the electrolyte that has been widely used for ORR characterizations, has a quite strong poisoning effect on the Fe-N-C catalysts. As indicated by the CV testing results shown in Fig. 4, the origin of this poisoning effect is likely the adsorption of specific anions on the active sites, i.e. FeN_x structure according to the current understanding [14,52]. In contrast to the case of Pt/C, such adsorption might not be strong enough to severely affect the rate-limiting step of ORR on the catalyst, reflected by the almost unchanged Tafel slopes obtained in the four electrolytes (Fig. S2 and Table S1). To fully understand the mechanism of anion adsorption on FeN_x sites, further exploration through experimental and computational studies is highly needed. Regarding the low catalyst activity in $HClO_4$, it should be mentioned that the origin of chloride from the possible electrochemical reduction of ClO_4^- at sufficiently low potentials has been considered as some metals such as Rh were reported to catalyze this reaction. [53,54] In the present CV tests of the catalyst in Ar-saturated $HClO_4$, however, no reductive peaks in the potential range of 0.1–1.0 V have been observed, as shown in Fig. 4. Furthermore, freshly prepared electrolytes were always used for every test and the ORR curves were recorded within several minutes. It is hence concluded that this effect should be very trivial if any.

Since the catalyst shows a negligible poisoning effect in H_3PO_4, it could be a good catalyst for high-temperature PEMFCs, where concentrated H_3PO_4 distributes throughout the electrodes. Before putting the catalyst into a fuel cell to test, we first checked the effect of H_3PO_4 concentration on the ORR performance of the catalyst. Fig. 5 shows the ORR curves of both Pt/C and BP-FeNC in H_3PO_4 of different concentrations. We can see the kinetic region of ORR curves for Pt/C (0.8–1.0 V) shift negatively with increasing the H_3PO_4 concentration, and the H_2O_2 yields become higher, both indicating the stronger adsorption effect in more concentrated H_3PO_4. While for BP-FeNC, the ORR curves don't show an obvious shift in the kinetic region (0.85–0.95 V), and the H_2O_2 yields are even slightly lower in more concentrated H_3PO_4, confirming the negligible poisoning effect of phosphate anions on the BP-FeNC catalyst. In 5.0 M (i.e., 30.4 wt%) H_3PO_4, the activity of the BP-FeNC has become higher than that of 20 wt% Pt/C (Fig. 5a).

At last, high-temperature PEMFC tests were conducted for a demonstration. Polarization curves of single cell high-temperature-PEMFC tests with 60 wt % Pt/C, 20 wt % Pt/C and BP-FeNC as the cathode catalyst are shown in Fig. 6. Using 60 wt % Pt/C, the cell shows a quite standard performance with the current density of 585.7 mA cm^{-2} at 0.60 V (Fig. 6) and the maximum power density of 700 mW cm^{-2} (Fig. S5).[8,55,56] With 20 wt % Pt/C, the overall cell performance was somewhat lower due to lower platinum loading. When BP-FeNC was employed, the cell performance was comparable to that with Pt/C electrodes, especially in the low but practically operational current

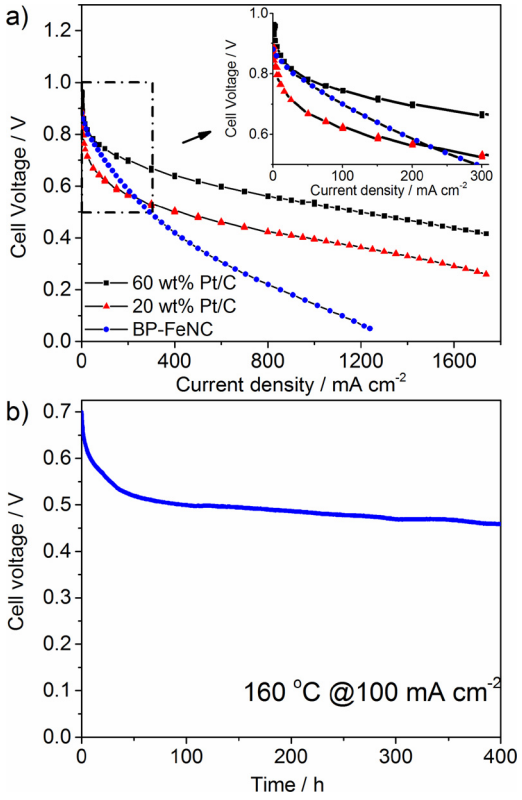

Fig. 6. a) Polarization curves of H_2-O_2 high-temperature PEMFC at ambient pressure and 160 °C with 60 wt% Pt/C (2.7 mg cm^{-2} or 1.6 mg$_{Pt}$ cm^{-2}), 20 wt% Pt/C (4.4 mg cm^{-2} or 0.9 mg$_{Pt}$ cm^{-2}), and BP-FeNC (7.8 mg cm^{-2}) as the cathode catalyst without iR correction (see Experimental section and Table 1 for the details). b) 400-hour durability test of H_2-O_2 HT-PEFMC at 100 mA cm^{-2} with BP-FeNC as the cathode catalyst. Constant current density operation was employed in the test to keep a constant λ (the ratio between the reactant feed and reactant consumption).

density range (> 0.6 V). The peak power density was 184.6 mW cm^{-2}(Fig. S5), and the current density at 0.6 V reached 189.2 mA cm^{-2} (Fig. 6). To the best of our knowledge, it is the highest performance ever reported for a high-temperature PEFMC using a NPMC in the cathode [57]. The stability of BP-FeNC was tested by operation of the HT-PEMFC at a constant current density of 100 mA cm^{-2}. As presented in Fig. 4b, the cell voltage shows a relatively fast decay (28.6% of the initial value) during the first 50 h of operation, after which the performance become quite stable with a further loss of only 5.4% in 350 h. Catalyst degradation or/and acid flooding in the electrode might be the reason for the performance decay. To fully understand the mechanism, however, more effort is needed and is in progress in our lab.

4. Conclusions

In summary, we have investigated the effect of four common anions (ClO_4^-, HSO_4^-, $H_2PO_4^-$, and Cl^-)on the ORR performance of a typical Fe-N-C catalyst. The catalyst was synthesized via a high-pressure pyrolysis in the presence of carbon support. As thoroughly characterized, it contained uniformly distributed FeN_x functionalities but had no metal particles. When tested in pH 1.0 $HClO_4$, H_2SO_4, H_3PO_4 or HCl solution, the catalyst showed an ORR activity (at 0.8 V vs. RHE) that decreased in the order of H_3PO_4 (8.6 mA mg^{-1}) > H_2SO_4 (5.3 mA mg^{-1}) > $HClO_4$ (3.1 mA mg^{-1}) > HCl (0.7 mA mg^{-1}). The same tests with a commercial Fe-N-C catalyst (NPC-2000 from Pajarito Powder) showed similar results. The poisoning effect observed in H_2SO_4, $HClO_4$, as well as HCl, is attributed to the strong adsorption of the acid anions on the active sites of the catalyst, as further confirmed by tests with varied ClO_4^- concentrations. This finding is of special significance by considering the fact that $HClO_4$ has been widely used in ORR tests of Fe-N-C catalysts. On the other hand, the catalyst showed a negligible poisoning effect in H_3PO_4, even in the concentrated form of 30.4 wt%. It suggests an obvious application of the type of NPMC in high-temperature PEMFCs, where concentrated H_3PO_4 distributes throughout the electrodes. As demonstrated, the catalyst did show excellent performance in high-temperature PEFMC tests, comparable to Pt/C catalysts.

Acknowledgements

We gratefully acknowledge financial support from the Danish ForskEL program (UPCAT, 2015-1-12315) and Innovation Fund Denmark (4M Centre, 12-132710 and NonPrecious, 4106-00012B).

Appendix A. Supplementary data

Supplementary material related to this article can be found, in the online version, at doi:https://doi.org/10.1016/j.apcatb.2018.03.056.

References

[1] http://money.cnn.com/2017/07/26/autos/countries-that-are-banning-gas-cars-for-electric/index.html.
[2] https://www.bloomberg.com/news/articles/2017-09-10/china-s-fossil-fuel-deadline-shifts-focus-to-electric-car-race-j7fktx9z.
[3] M.K. Debe, Electrocatalyst approaches and challenges for automotive fuel cells, Nature 486 (2012) 43–51.
[4] A. Rabis, P. Rodriguez, T.J. Schmidt, Electrocatalysis for polymer electrolyte fuel cells: recent achievements and future challenges, ACS Catal. 2 (2012) 864–890.
[5] H.A. Gasteiger, N.M. Markovic, Just a dream-or future reality? Science 324 (2009) 48–49.
[6] B.C.H. Steele, A. Heinzel, Materials for fuel-cell technologies, Nature 414 (2001) 345–352.
[7] J. Zhang, Z. Xie, J. Zhang, Y. Tang, C. Song, T. Navessin, Z. Shi, D. Song, H. Wang, D.P. Wilkinson, Z.-S. Liu, S. Holdcroft, High temperature PEM fuel cells, J. Power Sources 160 (2006) 872–891.
[8] A. Chandan, M. Hattenberger, A. El-kharouf, S. Du, A. Dhir, V. Self, B.G. Pollet, A. Ingram, W. Bujalski, High temperature (HT) polymer electrolyte membrane fuel cells (PEMFC) – a review, J. Power Sources 231 (2013) 264–278.
[9] Y. Nie, L. Li, Z. Wei, Recent advancements in Pt and Pt-free catalysts for oxygen reduction reaction, Chem. Soc. Rev. 44 (2015) 2168–2201.
[10] F. Jaouen, E. Proietti, M. Lefevre, R. Chenitz, J.-P. Dodelet, G. Wu, H.T. Chung, C.M. Johnston, P. Zelenay, Recent advances in non-precious metal catalysis for oxygen-reduction reaction in polymer electrolyte fuel cells, Energy Environ. Sci. 4 (2011) 114–130.
[11] Z. Chen, D. Higgins, A. Yu, L. Zhang, J. Zhang, A review on non-precious metal electrocatalysts for PEM fuel cells, Energy Environ. Sci. 4 (2011) 3167–3192.
[12] Z.H. Xia, L. An, P.K. Chen, D.G. Xia, Non-Pt nanostructured catalysts for oxygen reduction reaction: synthesis, catalytic activity and its key factors, Adv. Energy Mater. 6 (2016).
[13] M. Shao, Q. Chang, J.-P. Dodelet, R. Chenitz, Recent advances in electrocatalysts for oxygen reduction reaction, Chem. Rev. 116 (2016) 3594–3657.
[14] H.T. Chung, D.A. Cullen, D. Higgins, B.T. Sneed, E.F. Holby, K.L. More, P. Zelenay, Direct atomic-level insight into the active sites of a high-performance PGM-free ORR catalyst, Science 357 (2017) 479–484.
[15] J. Shui, C. Chen, L. Grabstanowicz, D. Zhao, D.-J. Liu, Highly efficient nonprecious metal catalyst prepared with metal–organic framework in a continuous carbon nanofibrous network, Proc. Natl. Acad. Sci. 112 (2015) 10629–10634.
[16] M. Lefevre, E. Proietti, F. Jaouen, J.P. Dodelet, Iron-based catalysts with improved oxygen reduction activity in polymer electrolyte fuel cells, Science 324 (2009) 71–74.
[17] E. Proietti, F. Jaouen, M. Lefevre, N. Larouche, J. Tian, J. Herranz, J.-P. Dodelet, Iron-based cathode catalyst with enhanced power density in polymer electrolyte membrane fuel cells, Nat. Commun. 2 (2011).
[18] S.K. Zecevic, J.S. Wainright, M.H. Litt, S.L. Gojkovic, R.F. Savinell, Kinetics of O 2 reduction on a Pt electrode covered with a thin film of solid polymer electrolyte, J. Electrochem. Soc. 144 (1997) 2973–2982.
[19] V. Stamenkovic, T.J. Schmidt, P.N. Ross, N.M. Markovic, Surface composition effects in electrocatalysis: Kinetics of oxygen reduction on well-defined Pt3Ni and Pt3Co alloy surfaces, J. Phys. Chem. B 106 (2002) 11970–11979.
[20] M. Nesselberger, S. Ashton, J.C. Meier, I. Katsounaros, K.J.J. Mayrhofer, M. Arenz, The particle size effect on the oxygen reduction reaction activity of Pt catalysts: influence of electrolyte and relation to single crystal models, J. Am. Chem. Soc. 133 (2011) 17428–17433.
[21] T.J. Schmidt, U.A. Paulus, H.A. Gasteiger, R.J. Behm, The oxygen reduction reaction on a Pt/carbon fuel cell catalyst in the presence of chloride anions, J. Electroanal. Chem. 508 (2001) 41–47.

[22] N. Markovic, P.N. Ross, The effect of specific adsorption of ions and underpotential deposition of copper on the electro-oxidation of methanol on platinum single-crystal surfaces, J. Electroanal. Chem. 330 (1992) 499–520.
[23] N. Markovic, M. Hanson, G. McDougall, E. Yeager, The effects of anions on hydrogen electrosorption on platinum single-crystal electrodes, J. Electroanal. Chem. Interfacial Electrochem. 214 (1986) 555–566.
[24] A. Berná, V. Climent, J.M. Feliu, New understanding of the nature of OH adsorption on Pt(111) electrodes, Electrochem. Commun. 9 (2007) 2789–2794.
[25] G.E. Dima, A.C.A. de Vooys, M.T.M. Koper, Electrocatalytic reduction of nitrate at low concentration on coinage and transition-metal electrodes in acid solutions, J. Electroanal. Chem. 554–555 (2003) 15–23.
[26] W.G. Pell, A. Zolfaghari, B.E. Conway, Capacitance of the double-layer at polycrystalline Pt electrodes bearing a surface-oxide film, J. Electroanal. Chem. 532 (2002) 13–23.
[27] R. Subbaraman, D. Strmcnik, V. Stamenkovic, N.M. Markovic, Three phase interfaces at electrified metal−solid electrolyte systems 1. Study of the Pt(hkl)−Nafion interface, J. Phys. Chem. C 114 (2010) 8414–8422.
[28] Q. Wang, Z.-Y. Zhou, Y.-J. Lai, Y. You, J.-G. Liu, X.-L. Wu, E. Terefe, C. Chen, L. Song, M. Rauf, N. Tian, S.-G. Sun, Phenylenediamine-based FeNx/C catalyst with high activity for oxygen reduction in acid medium and its active-site probing, J. Am. Chem. Soc. 136 (2014) 10882–10885.
[29] D. Malko, A. Kucernak, T. Lopes, Performance of Fe-N/C oxygen reduction electrocatalysts toward NO2-, NO, and NH2OH electroreduction: from fundamental insights into the active center to a new method for environmental nitrite destruction, J. Am. Chem. Soc. 138 (2016) 16056–16068.
[30] Y. Hu, J.O. Jensen, W. Zhang, L.N. Cleemann, W. Xing, N.J. Bjerrum, Q. Li, Hollow spheres of iron carbide nanoparticles encased in graphitic layers as oxygen reduction catalysts, Angew. Chem. Int. Ed. 53 (2014) 3675–3679.
[31] A. Chandan, M. Hattenberger, A. El-Kharouf, S.F. Du, A. Dhir, V. Self, B.G. Pollet, A. Ingram, W. Bujalski, High temperature (HT) polymer electrolyte membrane fuel cells (PEMFC) - a review, J. Power Sources 231 (2013) 264–278.
[32] M. Mamlouk, K. Scott, The effect of electrode parameters on performance of a phosphoric acid-doped PBI membrane fuel cell, Int. J. Hydrog. Energy 35 (2010) 784–793.
[33] Q. Li, G. Wu, D.A. Cullen, K.L. More, N.H. Mack, H.T. Chung, P. Zelenay, Phosphate-tolerant oxygen reduction catalysts, ACS Catal. 4 (2014) 3193–3200.
[34] Y.-J. Wang, N. Zhao, B. Fang, H. Li, X.T. Bi, H. Wang, Carbon-supported Pt-based alloy electrocatalysts for the oxygen reduction reaction in polymer electrolyte membrane fuel cells: particle size, shape, and composition manipulation and their impact to activity, Chem. Rev. 115 (2015) 3433–3467.
[35] U.I. Kramm, J. Herranz, N. Larouche, T.M. Arruda, M. Lefevre, F. Jaouen, P. Bogdanoff, S. Fiechter, I. Abs-Wurmbach, S. Mukerjee, J.P. Dodelet, Structure of the catalytic sites in Fe/N/C-catalysts for O-2-reduction in PEM fuel cells, Phys. Chem. Chem. Phys. 14 (2012) 11673–11688.
[36] G. Wu, C.M. Johnston, N.H. Mack, K. Artyushkova, M. Ferrandon, M. Nelson, J.S. Lezama-Pacheco, S.D. Conradson, K.L. More, D.J. Myers, P. Zelenay, Synthesis-structure-performance correlation for polyaniline-Me-C non-precious metal cathode catalysts for oxygen reduction in fuel cells, J. Mater. Chem. 21 (2011) 11392–11405.
[37] M.J. Fleige, G.K.H. Wiberg, M. Arenz, Rotating disk electrode system for elevated pressures and temperatures, Rev. Sci. Instrum. 86 (2015) 064101.
[38] D. Strmcnik, K. Kodama, D. van der Vliet, J. Greeley, V.R. Stamenkovic, N.M. Markovic, The role of non-covalent interactions in electrocatalytic fuel-cell reactions on platinum, Nat. Chem. 1 (2009) 466–472.
[39] D.V. Tripkovic, D. Strmcnik, D. van der Vliet, V. Stamenkovic, N.M. Markovic, The role of anions in surface electrochemistry, Faraday Discuss. 140 (2009) 25–40.
[40] T.M. Arruda, B. Shyam, J.M. Ziegelbauer, S. Mukerjee, D.E. Ramaker, Investigation into the competitive and site-specific nature of anion adsorption on pt using in situ X-ray absorption spectroscopy, J. Phys. Chem. C 112 (2008) 18087–18097.
[41] J.X. Wang, N.M. Markovic, R.R. Adzic, kinetic analysis of oxygen reduction on Pt (111) in acid solutions: Intrinsic kinetic parameters and anion adsorption effects, J. Phys. Chem. B 108 (2004) 4127–4133.
[42] N.M. Marković, P.N. Ross, Surface science studies of model fuel cell electrocatalysts, Surf. Sci. Rep. 45 (2002) 117–229.
[43] N.M. Marković, T.J. Schmidt, V. Stamenković, P.N. Ross, Oxygen reduction reaction on Pt and Pt bimetallic surfaces: a selective review, Fuel Cells 1 (2001) 105–116.
[44] A. Kolics, A. Wieckowski, Adsorption of bisulfate and sulfate anions on a Pt(111) electrode, J. Phys. Chem. B 105 (2001) 2588–2595.
[45] N.M. Markovic, H.A. Gasteiger, B.N. Grgur, P.N. Ross, Oxygen reduction reaction on Pt(111): effects of bromide, J. Electroanal. Chem. 467 (1999) 157–163.
[46] J. Perez, H.M. Villullas, E.R. Gonzalez, Structure sensitivity of oxygen reduction on platinum single crystal electrodes in acid solutions, J. Electroanal. Chem. 435 (1997) 179–187.
[47] N.M. Markovic, H.A. Gasteiger, P.N. Ross, Oxygen reduction on platinum low-index single-crystal surfaces in sulfuric acid solution: rotating ring-Pt(hkl) disk studies, J. Phys. Chem. 99 (1995) 3411–3415.
[48] F. El Kadiri, R. Faure, R. Durand, Electrochemical reduction of molecular oxygen on platinum single crystals, J. Electroanal. Chem. Interfacial Electrochem. 301 (1991) 177–188.
[49] Q. He, X. Yang, W. Chen, S. Mukerjee, B. Koel, S. Chen, Influence of phosphate anion adsorption on the kinetics of oxygen electroreduction on low index Pt(hkl) single crystals, Phys. Chem. Chem. Phys. 12 (2010) 12544–12555.
[50] Y.-H. Lee, K.-H. Chang, C.-C. Hu, Differentiate the pseudocapacitance and double-layer capacitance contributions for nitrogen-doped reduced graphene oxide in acidic and alkaline electrolytes, J. Power Sources 227 (2013) 300–308.
[51] M.S. Thorum, J.M. Hankett, A.A. Gewirth, Poisoning the oxygen reduction reaction on carbon-supported Fe and Cu electrocatalysts: Evidence for metal-centered activity, J. Phys. Chem. Lett. 2 (2011) 295–298.
[52] A. Zitolo, V. Goellner, V. Armel, M.-T. Sougrati, T. Mineva, L. Stievano, E. Fonda, F. Jaouen, Identification of catalytic sites for oxygen reduction in iron- and nitrogen-doped graphene materials, Nat. Mater. 14 (2015) 937–942.
[53] C.K. Rhee, M. Wasberg, G. Horanyi, A. Wieckowski, Strong anion surface interactions - perchlorate reduction on rh(100) electrode studied by voltammetry, J. Electroanal. Chem. 291 (1990) 281–287.
[54] M.Y. Rusanova, P. Polaskova, M. Muzikar, W.R. Fawcett, Electrochemical reduction of perchlorate ions on platinum-activated nickel, Electrochim. Acta 51 (2006) 3097–3101.
[55] Q.F. Li, J.O. Jensen, R.F. Savinell, N.J. Bjerrum, High temperature proton exchange membranes based on polybenzimidazoles for fuel cells, Prog. Polym. Sci. 34 (2009) 449–477.
[56] M. Mamlouk, K. Scott, An investigation of Pt alloy oxygen reduction catalysts in phosphoric acid doped PBI fuel cells, J. Power Sources 196 (2011) 1084–1089.
[57] Y. Hu, J.O. Jensen, W. Zhang, S. Martin, R. Chenitz, C. Pan, W. Xing, N.J. Bjerrum, Q. Li, Fe3C-based oxygen reduction catalysts: synthesis, hollow spherical structures and applications in fuel cells, J. Mater. Chem. A 3 (2015) 1752–1760.